Macromolecules
ARTICLE

Macromolecules **2009**, *42*, 9467–9480 **9467**
DOI: 10.1021/ma901740f

Nanostructure, Morphology, and Properties of Fluorous Copolymers Bearing Ionic Grafts

Emily M. W. Tsang,[†] Zhaobin Zhang,[†,§] Ami C. C. Yang,[†] Zhiqing Shi,[†,⊥] Timothy J. Peckham,[†] Rasoul Narimani,[‡] Barbara J. Frisken,[‡] and Steven Holdcroft*[,†]

[†]*Department of Chemistry, Simon Fraser University, Burnaby, BC V5A 1S6, Canada, and* [‡]*Department of Physics, Simon Fraser University, Burnaby, BC V5A 1S6, Canada.* [§] *Current address: BASF Auxiliary Chemicals Co., Ltd, 300 Jiang Xin Sha Road, Pudong, Shanghai 200137, China.* [⊥] *Current address: Institute for Fuel Cell Innovation, National Research Council Canada, 3250 East Mall, Vancouver, BC V6T 1W5, Canada.*

Received August 4, 2009; Revised Manuscript Received November 6, 2009

ABSTRACT: In order to probe the effects of polymer microstructure on the properties of proton conducting polymer membranes, three series of fluorous−ionic graft copolymers, partially sulfonated poly([vinylidene difluoride-*co*-chlorotrifluoroethylene]-*g*-styrene) [P(VDF-*co*-CTFE)-*g*-SPS], comprising controlled graft lengths and degrees of sulfonation were synthesized. The parent building block was a poly(vinylidene difluoride-*co*-chlorotrifluoroethylene) [P(VDF-*co*-CTFE)] macroinitiator ($M_n = 3.12 \times 10^5$ g/mol) synthesized to contain 1 chloro group per 17 repeat units, onto which polystyrene, having degrees of polymerization of 35, 88, and 154 units per graft, was grown by atom transfer radical polymerization (ATRP). These graft copolymers, termed *short*, *medium*, and *long* graft chains, were sulfonated to different extents to provide a series of polymers with varying ion exchange capacity (IEC). The resulting P(VDF-*co*-CTFE)-*g*-SPS copolymers were cast into proton exchange membranes, and their nanostructure, morphology, and properties were studied. TEM revealed that all three membrane series exhibit a disordered phase-separated morphology comprised of small interconnected ionic clusters varying from 2 to 4 nm in size. For a given IEC, membranes prepared from the short graft chain series possessed larger ionic domains due to their relatively higher degree of sulfonation (DS), which facilitates ion clustering. For short graft membranes, water contents and conductivities were less influenced by IEC. For high IEC membranes, ∼2.50 mmol/g, the short grafts remained water-insoluble, absorbed less water, and afforded higher conductivity than longer graft analogues. These results demonstrate the importance of polymer microstructure on the morphology of membranes, the size of ionic clusters and their ionic purity, and the microstructure's role in water sorption and proton conductivity. From a technological viewpoint, it indicates that short ionic graft polymers enhance the elastic forces in the matrix and inhibit excessive swelling, allowing high IEC vinylic polymers to remain insoluble. As such, these architectures warrant further investigation as they reduce swelling and promote proton transport under reduced lambda values.

Introduction

The material requirements for a proton exchange membrane (PEM) for application in fuel cells include (1) high proton conductivity, (2) long-term chemical stability, (3) good mechanical strength, (4) low gas (fuel, oxidant) permeability and high water transport properties, (5) interfacial compatibility with catalyst layer, and (6) from the commercial viewpoint, low production cost.[1−3] Perfluorosulfonic acid (PFSA) membranes, in particular Nafion, have been at the forefront of PEM development, offering to date the adequate combination of performance, durability, and reliability.[3,4] However, as the technological requirements for high volume commercialization of PEMFCs become increasingly stringent, Nafion membranes, having high cost and poor performances at high temperature (> 80 °C) and low relative humidity (< 40% RH),[2] are becoming less attractive. Over the past decade, significant research effort has been devoted to the design of alternate membrane materials with the intention of improving properties and lowering cost.[2−7] A wide variety of different polymer systems have been examined including perfluorinated ionomers,[5,8] partially fluorinated ionomers,[9−14] polystyrene-based systems,[15−22] poly(arylene ether)s,[23−28] polyimides,[29−33] polybenzimidazoles,[34−37] and polyphosphazenes.[38−41] Despite this growing body of research, there exists a void in our understanding of fundamental structure−property relationships of PEMs in terms of the role of microstructure on morphology and the role of morphology on a membrane's property.

In addition to the polymer's chemical structure, i.e., its composition, microstructure, sequence distribution, nature of the acid group, and ion content, the membrane's nanostructure and morphology play a profound role in the proton conduction.[42,43] The microstructure of Nafion membrane has been extensively studied using both small-angle X-ray (SAXS) and neutron scattering (SANS).[44−47] Interconnected, nanometer-sized ionic channels are believed to form due to phase separation between the incompatible hydrophobic polymer backbone and hydrophilic sulfonic acid groups. Proton conduction occurs through these hydrophilic channels, mediated by water that is either strongly associated with the acidic groups or present as bulk water in the channels.[44,47,48] However, there is yet a clear understanding of how polymer architecture influences aggregation and connectivity of ionic domains and thereby morphology and conductivity. In this regard, model polymer systems, in which

*To whom correspondence should be addressed. E-mail: holdcrof@sfu.ca.

© 2009 American Chemical Society
Published on Web 11/24/2009

polymer architectures can be controlled and systematically studied, are essential both for elucidating relationships between structure, morphology, and ionic conductivity and for obtaining insights into structural preferences for proton conductivity.

The approach of using model polymers for investigating structure−property relationships in PEMs is a core focus of our group.[43,49−64] Our earlier work, aimed at controlling membrane morphology, involved a novel class of well-defined graft polymers comprising styrenic main chain and sodium styrenesulfonate graft chains (PS-*g*-macPSSNa).[62,63] These graft copolymers, prepared by copolymerization of styrene and macromonomers of poly(sodium styrenesulfonate) (macPSSNa), are amphiphilic, forming ionic aggregates in a hydrophobic matrix. Comparisons between the more structurally ordered PS-*g*-macPSSNa and random copolymers of styrene and SSNa (PS-*r*-SSNa) revealed that structural order gave rise to significantly higher proton conductivity. TEM analysis revealed that PS-*g*-macPSSNa membranes exhibited clear signs of nanophase separation and a continuous network of ionic channels, whereas PS-*r*-PSSNa was lacking in phase separation. These results provided early, unambiguous evidence that proton conductivity can be greatly influenced by a membrane's microstructure.

More recently, we reported diblock systems of partially sulfonated poly([vinylidene difluoride-*co*-hexafluoropropylene]-*b*-styrene) [P(VDF-*co*-HFP)-*b*-SPS] possessing a hydrophobic fluorous segment linearly attached to a hydrophilic sulfonated styrene segment,[56,57] based on the knowledge that semifluorous block copolymers combine the self-organizational characteristics of block copolymers and the unique properties of fluoropolymers.[65,66] These amphiphilic fluorous−ionic diblock copolymers were found to display varying degrees of nanophase separation dependent upon the ion content (IEC) of the styrene block. For 0.9−1.2 mmol/g IEC membranes, distinct perforated lamellae were observed. Proton conductivities (0.06−0.08 S/cm) are comparable to Nafion and, moreover, higher than random copolymers of styrene and styrenesulfonic acid (PS-*r*-PSSA) as well as other non-fluorous styrene-containing block copolymers, such as sulfonated poly(styrene-*b*-[ethylene-*co*-butylene]-*b*-styrene) [S-SEBS] and sulfonated hydrogenated poly(butadiene-*b*-styrene) [S-HPBS], because the fluorous blocks in sulfonated copolymers promote phase separation.[58,59]

Zhang and Russell[67] recently reported partially fluorinated graft copolymers of poly([vinylidene difluoride-*co*-chlorotrifluoroethylene]-*g*-styrene) [P(VDF-*co*-CTFE)-*g*-PS] prepared by graft-atom transfer radical polymerization (g-ATRP) of styrene from commercial P(VDF-*co*-CTFE). This "grafting-from" method allows good control of polymer architecture compared to the conventional irradiation[68,69] or ozone[70,71] mediated free radical polymerization routes. The idea that fluorous/styrenic block copolymers can readily be converted into proton conducting electrolytes by postsulfonation of the styrene block provides further impetus for investigating this polymer system.

We recently reported the preparation of proton conducting partially sulfonated P(VDF-*co*-CTFE)-*g*-SPS graft copolymers by g-ATRP of styrene from P(VDF-*co*-CTFE) macroinitiators followed by postsulfonation.[52] In terms of chemical composition, these P(VDF-*co*-CTFE)-*g*-SPS graft copolymers (Figure 1) are similar to the previously studied P(VDF-*co*-HFP)-*b*-SPS diblock copolymers,[56,57] as they both contain fluorous and partially sulfonated polystyrene segments. Yet, they possess very distinctive microstructure: P(VDF-*co*-CTFE)-*g*-SPS contains a hydrophobic fluorous backbone with ionic sulfonated styrenic side chains whereas P(VDF-*co*-HFP)-*b*-SPS possesses a hydrophobic segment linearly attached to an ionic sulfonate styrenic segment. A direct comparison between these graft and diblock systems was recently reported for the purpose of obtaining insights into aspects of preferred polymer architecture.[52] It was found that

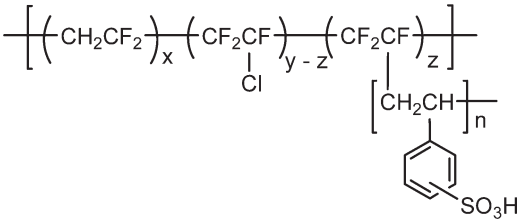

Figure 1. Chemical structure of P(VDF-*co*-CTFE)-*g*-SPS graft copolymers.

the morphology and properties of the membranes are highly dependent upon the polymer architecture. The P(VDF-*co*-HFP)-*b*-SPS diblock membranes, exhibiting long-range perforated lamellar morphologies, showed relatively higher proton conductivity for IECs ranging from 0.7 to 1.3 mmol/g; however, this long-range ionic order led, ironically, to excessive swelling and loss of mechanical integrity at IEC > 1.3 mmol/g. In contrast, the graft copolymers yielded membranes with an interconnected network of small ionic clusters (2−3 nm in size), similar in shape but smaller than those in Nafion (5−10 nm in size). These graft membranes were more resistant to excessive swelling in water and thus were able to maintain high proton conductivity (0.078−0.093 S/cm) and mechanical strength with high ion content (IEC 2.0−2.2 mmol/g). In addition, the isotropic nature of the ionic cluster network in the graft membranes led to more isotropic proton conduction.

Because of these intriguing results, the P(VDF-*co*-CTFE)-*g*-SPS graft system is attracting more attention. They serve as model systems for studying structure−property relationships because their composition and microstructure can be systematically varied by control of graft length, graft density, degree of sulfonation, and IEC. Recently, Chung et al.[72] reported the synthesis of P(VDF-*co*-CTFE)-*g*-SPS which revealed the effects of polymer microstructures, namely, molecular weight of the polymer backbone and graft density, on membrane properties. Two families of P(VDF-*co*-CTFE)-*g*-SPS graft copolymers, based on a low (M_n = ∼20 000 g/mol) and a high (M_n = 312 000 g/mol) molecular weight P(VDF-*co*-CTFE), having different graft density, graft length, and sulfonation levels, were systemically prepared. It was found that graft copolymers possessing low graft density (0.3−0.8 mol %) and long SPS graft length ($DP_{styrene}$ = 70−120) formed a well-microphase-separated morphology with long-range ionic channels (lamellar/cylindrical) imbedded in a highly crystalline fluorocarbon matrix. Although this morphology exhibited a lower percolation threshold and lower activation energy for proton conduction, the authors note it also led to increased water swelling and a high sensitivity to humidity. On the other hand, graft copolymers with higher graft density (1.4−2.4 mol %) and short SPS graft length ($DP_{styrene}$ = 10−30) gave rise to a disordered cluster network morphology with small cluster size, consistent with that previously reported.[52] This morphology resulted in a higher resistance to water swelling, less sensitivity to humidity, relatively improved performance under low RH conditions, and increased conductivity at higher temperatures. In addition, it was also reported that a high molecular weight P(VDF-*co*-CTFE) backbone resulted in smaller ionic channel width, lower water uptake, and enhanced resistance to excessive water swelling at high IEC ranges.

These studies on P(VDF-*co*-CTFE)-*g*-SPS graft systems warrant further investigation to determine whether a combination of high molecular weight P(VDF-*co*-CTFE) backbone and high graft density lead to membranes with cluster network morphologies that reduce the propensity of water swelling even further and to determine whether such cluster network morphologies can be further correlated to microstructure. An important question that remains unanswered is the preference of having larger, but

Scheme 1. Structure Relationship between the Various Series of P(VDF-*co*-CTFE)-*g*-SPS

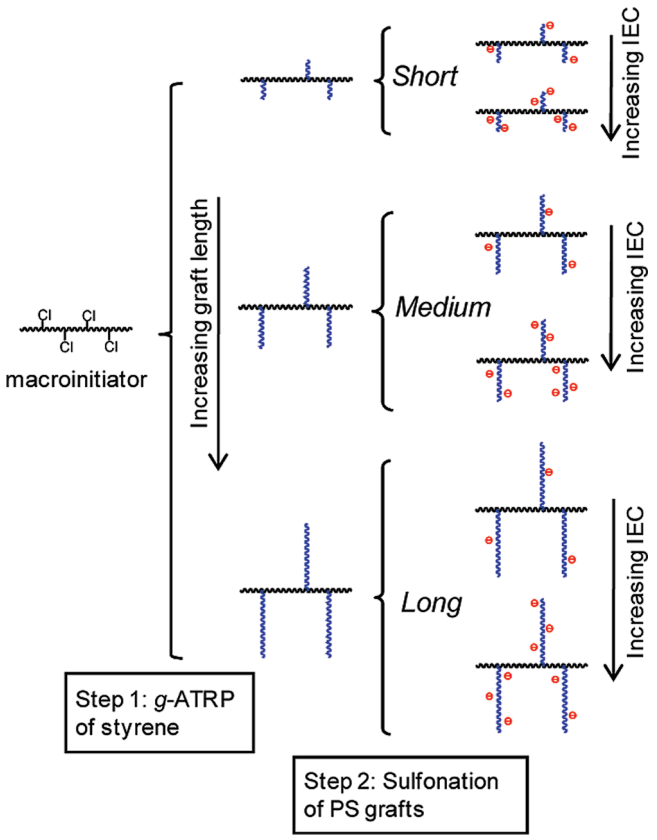

widely spaced, ionic clusters or smaller, but closely spaced, ionic clusters imbedded in a hydrophobic fluorocarbon matrix. For the P(VDF-*co*-CTFE)-*g*-SPS system, the length of the sulfonated polystyrene grafts (SPS), in principle, would influence the size of the ionic clusters. In order to manipulate the ionic cluster size without changing the overall cluster network morphology, it is important that the SPS graft length is varied while the graft density is kept constant.

In this paper, we synthesize P(VDF-*co*-CTFE)-*g*-SPS in order to elucidate the effects of SPS graft length—at a *fixed* graft density—on membrane morphology and membrane properties. Three parent copolymers of P(VDF-*co*-CTFE)-*g*-PS, with similar graft density (~2.5 mol %) but different PS graft length ($DP_{styrene}$ = 35, 88, 154), were prepared. Each parent P(VDF-*co*-CTFE)-*g*-PS copolymer was sulfonated to different extents to provide a series of ionic P(VDF-*co*-CTFE)-*g*-SPS, which were cast into membranes to provide families of membranes with varying ion exchange capacity. The structural variations in the three series of graft copolymers are shown in Scheme 1. The correlation between graft length, morphology, and properties such as proton conductivity, proton mobility, proton concentration, water uptake, and crystallinity reveal interesting trends that are counterintuitive but important in the design of next-generation proton conducting membranes.

Experimental Section

Materials. Vinylidene difluoride (VDF, Aldrich, 99+%), chlorotrifluoroethylene (CTFE, Aldrich, 98%), potassium persulfate (KPS, Allied Chemical, reagent grade), sodium metabisulfite ($Na_2S_2O_5$, Anachemia, anhydrous, reagent grade), pentadecafluorooctanoic acid (Aldrich, 96%), copper(I) chloride (CuCl, Aldrich, 99%), copper(II) chloride ($CuCl_2$, Aldrich, 99.999%), 2,2′-dipyridyl (bpy, Aldrich, 99+%), 1,2-dichloroethane (Caledon, reagent grade), *N*-methyl-2-pyrrolidone (NMP, Aldrich, anhydrous, 99.5%), *N,N*-dimethylacetamide (DMAc, Aldrich, anhydrous, 99.8%), sulfuric acid (Anachemia, 95−98%, ACS reagent), and acetic anhydride (Aldrich, 99.5%) were used as received. Styrene (St, Aldrich, 99+%) was washed twice with aqueous 5% NaOH and twice with water, dried overnight with $MgSO_4$, distilled over CaH_2 under reduced pressure, and stored under N_2 at −20 °C.

Synthesis of Fluorous Macroinitiator [P(VDF-*co*-CTFE)]. The macroinitiator was prepared by emulsion copolymerization of vinylidene difluoride (VDF) and chlorotrifluoroethylene (CTFE) as follows: to a 160 mL pressure vessel (Parr Instruments) equipped with a 600 psi pressure relief valve and a magnetic stir bar, a mixture of 100 mL of water, 0.40 g of KPS, 0.29 g of $Na_2S_2O_5$, and 0.04 g of pentadecafluorooctanoic acid was added. A monomer mixture (VDF and CTFE) with a predetermined composition was then introduced into the reactor. The polymerization was carried out for 1 h at 60 °C, and a constant pressure of 300 psi was maintained by resupplying the vessel with the monomer mixture. The resulting polymer latex was coagulated by freezing, followed by washing with water and ethanol. The crude fluoropolymer was purified by repeated dissolution in THF and reprecipitation in ethanol. The sample was dried at 80 °C under vacuum for 24 h. ^{1}H NMR (500 MHz, d_6-acetone) δ (ppm): 2.75−3.30 ($-CF_2-CH_2-CF_2-\mathbf{CH_2}^*-CF_2-CH_2-$), 2.15−2.45 ($-CH_2-CF_2-CF_2-\mathbf{CH_2}^*-CH_2-CF_2-$). ^{1}F NMR (400 MHz, d_6-acetone) δ (ppm): −90.0 − −94.0 ($-CF_2-CH_2-\mathbf{CF_2}^*-CH_2-CF_2-$), −95.1 ($-CF_2-CH_2-\mathbf{CF_2}^*-CH_2-CH_2-$), −108.7 ($-CF_2-CH_2-\mathbf{CF_2}^*-CF_2-CFCl-$), −114.2 ($-CF_2-CH_2-\mathbf{CF_2}^*-CF_2-CH_2-$), −116.6 ($-CH_2-CF_2-\mathbf{CF_2}^*-CFCl-CF_2-$), −118.5 to −120.0 ($-CH_2-CF_2-\mathbf{CF_2}^*-CFCl-CH_2-$), −120.0 to −121.4 ($-CF_2-CF_2-\mathbf{CF^*Cl}-CH_2-CF_2-$). The composition of the P(VDF-*co*-CTFE) macroinitiator was calculated by ^{19}F NMR according to published methods[73] and found to be 5.8 ± 0.3 mol % CTFE and 94.2 ± 0.3 mol % VDF.

Grafting ATRP of Styrene onto P(VDF-*co*-CTFE) Macroinitiator. The P(VDF-*co*-CTFE) macroinitiator (1.0 g, $M_n = 3.12 \times 10^3$ Da) was dissolved in NMP (40 mL) at 60 °C in a dried flask equipped with a rubber septum and a magnetic stirring bar. After cooling to room temperature, CuCl (0.65 g, 6.5 mmol), $CuCl_2$ (0.09 g, 0.66 mmol), bpy (3.0 g, 19.2 mmol), and styrene (20 mL, 174.6 mmol) were added. Three freeze−pump−thaw cycles were performed to remove oxygen. The polymerization reaction was carried out at 110 °C under a nitrogen blanket. Polymer samples were periodically removed from the reaction flask using a syringe after 8, 16, and 24 h. The polymer samples were diluted with THF, purified by passing through a column of alumina, and then precipitated into methanol. Homopolymer of polystyrene was removed by washing repeatedly with cyclohexane. The resulting P(VDF-*co*-CTFE)-*g*-PS copolymers were dried under vacuum at 60 °C. ^{1}H NMR (500 MHz, d_6-acetone) δ (ppm): 6.35−7.30 (aryl), 2.80−3.10 (methylene, head-to-tail VDF sequences), 2.05−2.50 (methylene, head-to-head or tail-to-tail VDF sequences), 1.80−2.10 (benzylic), 1.10−1.80 (methylene, styrene). The ^{19}F NMR spectrum of P(VDF-*co*-CTFE)-*g*-PS showed similar signature peaks to that of the fluorous macroinitiator described above, except an additional peak at −165 ppm ($-CF_2-C\mathbf{F}^*[CH_2CH(C_6H_5)]_n-CF_2-$).

Sulfonation of Polystyrene Graft Chains. Sulfonation was carried out in 1,2-dichloroethane using a procedure described in the literature,[74] except a reaction temperature of 40 °C was used. A typical sulfonation reaction is as follows: to a 50 mL three-neck flask equipped with a dropping funnel and condenser, P(VDF-*co*-CTFE)-*g*-PS (0.6 g) and 1,2-dichloroethane (15 mL) were added. The mixture was heated to 50 °C under N_2 and stirred until complete dissolution. Acetyl sulfate was prepared by injecting acetic anhydride (1 mL) and 1,2-dichloroethane (3 mL) into a nitrogen-purged vial. The solution was cooled to 0 °C in a 10% $CaCl_2$ ice bath, after which 95−97% sulfuric acid (0.3 mL) was added. The resultant acetyl sulfate was immediately added to the polymer solution at 40 °C using a dropping funnel. Samples sulfonated

to various degrees were periodically extracted and precipitated in ethanol/hexanes (50/50 by volume). The precipitate was washed repeatedly with water until the residual water was pH 7. The partially sulfonated P(VDF-*co*-CTFE)-*g*-SPS was dried under vacuum at 60 °C overnight. The ^{1}H NMR spectrum of P(VDF-*co*-CTFE)-*g*-SPS showed similar signature peaks to that of the pristine P(VDF-*co*-CTFE)-*g*-PS described above, except an additional peak at 7.60−7.30 ppm, corresponding to aromatic protons adjacent to the sulfonate group, was observed.

Membrane Preparation and Characterization. Membranes were prepared by dissolving the sulfonated graft copolymers in *N,N*-dimethylacetamide and casting on a leveled Teflon sheet. Polymer films were dried at ambient temperature for 2 days and then at 60 °C under vacuum overnight. The membranes (∼100 μm thick) were converted to the protonic form by immersing in 2 M HCl overnight. The protonated membranes were washed several times with deionized water for 30 min periods and placed in water overnight to remove excess acid on the surface and interior of the membranes.

The pretreated membranes (acidic form) were equilibrated in 2 M NaCl for 4 h to release the protons, which were subsequently titrated with 0.001 M NaOH to a phenolphthalein end point. Acid−base control titrations were performed on 2 M NaCl solutions with no membranes present to determine the blank titration volume. After titration, the membranes were immersed in 2 M HCl for a minimum of 4 h to reprotonate the sulfonic sites. After drying at 70 °C under vacuum overnight, the membranes' "dry" weight was measured. The ion exchange capacity (IEC, mmol/g) of the membrane was calculated by

$$\text{IEC} = \frac{V_{\text{NaOH}} M_{\text{NaOH}}}{W_{\text{dry}}} \tag{1}$$

where V_{NaOH} and M_{NaOH} are the blank-corrected volume (mL) and molar concentration (mol/L) of NaOH solution, respectively. W_{dry} is the dry weight of the membrane.

The membranes were equilibrated in deionized water overnight at room temperature and blotted with a Kimwipe to remove surface water prior to determining the "wet" weight. The water uptake was calculated as the percentage increase in mass over the "dry" weight and given by

$$\text{water uptake} = \frac{W_{\text{wet}} - W_{\text{dry}}}{W_{\text{dry}}} \times 100\% \tag{2}$$

where W_{wet} and W_{dry} are the wet and dry weight of the membrane, respectively.

The water content was calculated both as a mass and a volume percentage of water in the "wet" membrane and given by

$$\text{water content (wt \%)} = \frac{W_{\text{wet}} - W_{\text{dry}}}{W_{\text{wet}}} \times 100\% \tag{3}$$

$$\text{water content (vol \%)} = X_{\text{v}} = \frac{\text{Vol}_{\text{wet}} - \text{Vol}_{\text{dry}}}{\text{Vol}_{\text{wet}}} \tag{4}$$

where Vol_{wet} and Vol_{dry} are the wet and dry volume of the membrane, respectively. The thickness was measured with Series 293 Mitutoyo Quickmike calipers while length and width were measured with Mitutoyo Digimatic calipers.

IEC, water uptake, and water content values were taken as the average values of five membrane samples.

Water uptake was also examined in terms of the average number of water molecules per ion exchange site ($[H_2O]/[SO_3^-]$), often referred to as λ value, and was calculated by

$$[H_2O]/[SO_3^-] = \lambda = \frac{\text{water uptake (\%)} \times 10}{18 \times \text{IEC (mmol/g)}} \tag{5}$$

The analytical acid concentration in "wet" membrane was calculated by

$$[-SO_3H] = \frac{W_{\text{dry}}\ (\text{g})}{\text{Vol}_{\text{wet}}\ (\text{cm}^3)} \times \text{IEC (mmol/g)} \tag{6}$$

The *effective* proton mobility in "wet" membranes (μ_{eff}) was given by

$$\mu_{\text{eff}} = \frac{\sigma}{F[-SO_3H]} \tag{7}$$

where F is Faraday's constant and σ (S/cm) is the proton conductivity.

Instrumentation and Techniques. The molecular weight of the macroinitiator and the graft copolymers were estimated by gel permeation chromatography (GPC) using DMF (0.01 M LiBr) eluant, three Waters Styragel HT columns at 50 °C, a Waters 1515 isocratic HPLC pump, a Waters 2414 differential refractometer, and a Waters 2487 dual UV absorbance detector (λ = 254 nm). Polystyrene standards were used for calibration. ^{1}H NMR spectra (in d_6-acetone) were recorded on a 500 MHz Varian Inova spectrometer; ^{19}F NMR spectra (in d_6-acetone) were recorded on a 400 MHz Varian MercuryPlus spectrometer, and chemical shifts were measured with respect to trichlorofluoromethane ($CFCl_3$).

In-plane proton conductivity was measured by ac impedance spectroscopy with a Solartron 1260 frequency response analyzer (FRA) employing a two-electrode configuration, according to a procedure described elsewhere.[75] Briefly, a membrane (10 mm × 5 mm) was placed between two Pt electrodes of a conductivity cell, and a 100 mV sinusoidal ac voltage over a frequency range of 10 MHz−100 Hz was applied. The resulting Nyquist plots were fitted to the standard Randles equivalent circuit to determine the membrane resistance. Proton conductivity (σ) was calculated by

$$\sigma = \frac{L}{RA} \tag{8}$$

where L (cm) is the distance between electrodes, R (Ω) is the membrane resistance, and A (cm^2) is the cross-sectional area of the membrane. An ESPEC SH-241 temperature/humidity chamber was used for the measurement of membrane conductivity under conditions of variable temperature and humidity. Membranes were equilibrated overnight in the chamber at a predetermined temperature and relative humidity. Measurements were collected until a constant ionic resistance was obtained. All conductivity values reported were taken as average values of five membrane samples.

Samples for transmission electron microscopy (TEM) were prepared as follows: membranes were stained by soaking in a saturated lead acetate solution overnight, then rinsed in water, and dried under vacuum at room temperature for 4 h. The stained membranes were embedded in Spurr's epoxy and cured overnight in an oven at 60 °C. The samples were sectioned to yield slices 60−100 nm thick using a Leica UC6 ultramicrotome and picked up on copper grids. Electron micrographs were taken with a Hitachi H7600 TEM using an accelerating voltage of 100 kV. The size of the ionic domains was estimated using ImageJ software version 1.41, from National Institutes of Health. The domain sizes were reported as average over ∼100 measurements. The cluster number density in 2 dimensions was estimated by counting the number of ionic clusters present in a predetermined area, as follows: a 1 × 1 cm grid was overlaid on the TEM image, and the number of clusters present was counted in random sampling areas. The cluster number densities were reported as average over ∼30 samples and expressed in terms of number of clusters per 1000 nm^2.

Scheme 2. Synthetic Scheme for P(VDF-*co*-CTFE)-*g*-SPS

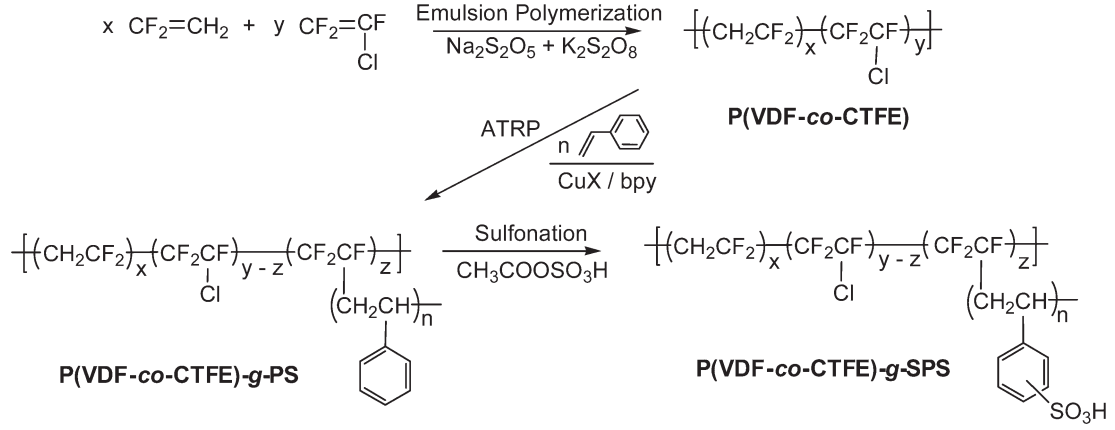

Table 1. Chemical Compositions of P(VDF-*co*-CTFE)-*g*-PS Parent Graft Copolymers

	P(VDF-*co*-CTFE)[a]	P(VDF-*co*-CTFE)-*g*-PS					
graft copolymer	g-ATRP reaction time (h)	$M_{n,GPC}$[b] (Da)	$M_{n,NMR}$[c] (Da)	St/VDF[d] (mole ratio)	% Cl reacted[e]	graft density[f]	graft length[g]
short	8	3.32×10^5	6.76×10^5	80/100	39	2.3	35
medium	16	3.95×10^5	13.6×10^5	230/100	44	2.6	88
long	24	4.48×10^5	22.0×10^5	415/100	46	2.7	154

[a] P(VDF-*co*-CTFE) macroinitiator: $M_{n,GPC} = 3.12 \times 10^5$ Da, 5.8 mol % CTFE. [b] Measured by DMF-GPC, calibrated with linear PS standards. [c] Calculated using the $M_{n,GPC}$ of P(VDF-*co*-CTFE) and the ratio of St/VDF from ^{1}H NMR. [d] Based on ^{1}H NMR. [e] Based on ^{19}F NMR. [f] Number of PS grafts per 100 units in fluorous backbone, calculated from the mol % of CTFE in P(VDF-*co*-CTFE) (5.8%) multiplied by the % of Cl reacted during g-ATRP. [g] Average number of styrene units in each graft, calculated from the St/VDF mole ratio divided by graft density.

Wide-angle X-ray scattering (WAXS) experiments were performed on a Siemens D-5000 diffractometer, using a Cu K α source ($\lambda = 0.154$ nm) at 50 kV and 30 mA. Membrane samples were maintained at ambient temperature and humidity, and data were collected over q range of 0.4−2.8 Å^{-1} in transmission mode.

Results and Discussion

Synthesis of P(VDF-*co*-CTFE)-*g*-SPS Graft Copolymers. Fluorous−ionic graft copolymers of P(VDF-*co*-CTFE)-*g*-SPS were prepared via a "grafting from" macroinitiator approach followed by postsulfonation, as illustrated in Scheme 2. To obtain the fluorous macroinitiator bearing chlorine sites for subsequent initiation of g-ATRP, chlorotrifluoroethylene (CTFE) was incorporated into the backbone by its emulsion copolymerization with vinylidene fluoride (VDF). The incorporation of large percentages of CTFE (> 10 mol %) led to cross-linking and gelation during subsequent graft polymerization reaction; it was thus necessary to control and reduce the CTFE content. A P(VDF-*co*-CTFE) copolymer ($M_{n,GPC}$ of 312 000 Da), containing 5.8 mol % of CTFE was prepared. To further inhibit cross-linking during g-ATRP, a small amount of a deactivator, $CuCl_2$ (5 mol % relative to CuCl), was introduced to the CuCl/bpy catalyst system. GPC traces of the P(VDF-*co*-CTFE) macroinitiator and the resulting P(VDF-*co*-CTFE)-*g*-PS graft copolymers at various reaction times were obtained (see Supporting Information, Figure S1). It is observed that after graft polymerization the initial negative RI signal of the macroinitiator transforms to a positive signal. In addition, as the reaction proceeds, the GPC traces shift to a higher molecular weight. These results are indicative of grafting of styrene onto the macroinitiator. The molecular weights of the resulting graft copolymers estimated by GPC ($M_{n,GPC}$) are listed in Table 1. In this graft system, monomer units are grown as side chains from multiple initiating sites along the backbone. Such branching architecture in a graft copolymer will lead to relatively smaller dynamic volume compared to a linear copolymer of the same molecular weight, thus causing M_n to be underestimated. A more accurate estimate of the graft polymers' molecular weight was obtained by ^{1}H NMR.

^{1}H NMR spectra of the P(VDF-*co*-CTFE) macroinitiator and the resulting P(VDF-*co*-CTFE)-*g*-PS graft copolymers were obtained (see Supporting Information, Figure S2). Peaks between 2.2 and 2.5 ppm (peak "a") are due to the head-to-head and tail-to-tail VDF sequences. Peaks at 2.8−3.3 ppm (peak "a") are due to the head-to-tail VDF sequences. These peaks are observed in both the macroinitiator and the resulting graft copolymers. However, additional peaks are found in the graft copolymers. Peaks at 1.10−1.80 and 1.80−2.10 ppm are due to the methylene and the benzylic protons of styrene, respectively. Peaks at 6.35−7.30 ppm (peaks "d" and "e") correspond to the aromatic protons of styrene. Quantification of the amount of styrene grafted onto the macroinitiator can be determined from the ratio of integrated signals due to the aromatic styrenic protons (peaks "d" and "e") and the methylene protons of VDF (peak "a"), as follows:

$$\frac{\text{St}}{\text{VDF}} = \frac{D+E}{A} \times \frac{2}{5} \tag{9}$$

where D, E, and A represent the integrals of "d", "e", and "a" peaks, respectively. As the reaction proceeds, the ratio of styrene to VDF increases. The molecular weights of P(VDF-*co*-CTFE)-*g*-PS estimated from ^{1}H NMR ($M_{n,NMR}$) are summarized in Table 1.

In order to estimate the average length of the polystyrene grafts, an estimate of the number density of PS grafts is required. The number of CTFE units involved in the g-ATRP reaction directly reflects the graft number density, and this can be determined using ^{19}F NMR (see Supporting Information, Figure S3). It is observed that the resulting

graft copolymers possessed similar ^{19}F NMR signature peaks to the macroinitiator, but an additional peak was found at −165 ppm (peak "d") due to tertiary fluorine atoms at carbon centers bearing a graft chain (−CF_2−**CF***[CH_2-$CH(C_6H_5)]_n$−CF_2−). Following g-ATRP, the peak centered at −121 ppm (peak "c"), corresponding to −**CF***Cl−, was reduced in intensity because a portion of the −CFCl units had reacted. The % of Cl sites initiating g-ATRP can be quantified by measuring the ratio of integrals for peak "d" and "c", as given by

$$\%\ \text{Cl reacted} = \frac{D}{D+C} \times 100\% \qquad (10)$$

where C and D represent the integrals of peaks "c" and "d", respectively. After 8 h it was found that 39% of all Cl groups had reacted. It was observed that as the reaction time was increased to 16 and 24 h, the number of sites reacted had increased marginally to 44 and 46%, respectively. The data represent graft densities of 2.3, 2.6, and 2.7 mol % for 8, 16, and 24 h reaction times, respectively. Using both the St/VDF ratio estimated from ^{1}H NMR and the graft number density estimated from ^{19}F NMR, the average degree of polymerization of styrene ($DP_{styrene}$) for the 8, 16, and 24 h reaction times was estimated to be 35, 88, and 154, respectively.

The experimental results and chemical compositions (i.e., M_n, St/VDF, graft number density, graft length, etc.) of the P(VDF-*co*-CTFE)-*g*-PS graft copolymers are summarized in Table 1. These graft copolymers were synthesized so as to possess very similar graft density (i.e., between 2.3 and 2.7 mol %) but different PS graft length in which the graft length was approximately doubled with each series. These are termed *short*, *medium*, and *long* graft lengths, respectively.

Each of the three P(VDF-*co*-CTFE)-*g*-PS copolymers was used as parent polymer for subsequent sulfonation. The sulfonation reactions were carried out to different extents to provide three series of partially sulfonated P(VDF-*co*-CTFE)-*g*-SPS polymers. NMR spectroscopy was used to quantify the degree of sulfonation (see Supporting Information, Figure S2). ^{1}H NMR spectra of partially sulfonated graft copolymers exhibit a peak at 6.80−7.30 ppm (peak "e") due to meta and para protons on the non-sulfonated phenyl rings. The peak at 7.30−7.60 ppm (peak "f") is assigned to aromatic protons adjacent to the sulfonate group on the sulfonated phenyl rings. The degree of sulfonation, represented as DS (%), was quantified using the ratio of integrals for peaks "e" and "f", as follows

$$\text{DS}\ (\%) = \frac{F/2}{F/2 + E/3} \times 100\% \qquad (11)$$

where E and F represent the integrals of peaks "e" and "f", respectively.

The macromolecular structural relationships between the three series of P(VDF-*co*-CTFE)-*g*-SPS polymers are illustrated in Scheme 1. From these polymers, three series of membranes processing similar graft number density, varying graft chain length, and varying ion exchange capacity (IEC) were prepared, which allowed the opportunity to systematically investigate the effects of graft chain lengths on membrane properties and morphology, as discussed in the next section. Compositional data for these membranes are summarized in Table 2.

TEM. Transmission electron micrographs (TEMs) of selected membranes prepared from the *short*, *medium*, and *long* graft length polymers are shown in Figure 2. To investigate phase separation and ionic aggregation, membranes were stained with lead acetate; thus, dark areas correspond to regions of high ionicity and brighter areas to

Table 2. P(VDF-*co*-CTFE)-*g*-SPS Graft Copolymer Membranes

series	membrane	graft density	graft length	DS (%)[a]	measured IEC[b]
short	S-1	2.3	35	13	0.64 ± 0.02
	S-2			21	1.03 ± 0.03
	S-3			26	1.22 ± 0.02
	S-4			34	1.59 ± 0.02
	S-5			44	1.98 ± 0.05
	S-6			59	2.48 ± 0.03
medium	M-1	2.6	88	10	0.73 ± 0.01
	M-2			15	1.02 ± 0.03
	M-3			18	1.22 ± 0.01
	M-4			21	1.40 ± 0.04
	M-5			26	1.67 ± 0.02
	M-6			34	2.10 ± 0.02
	M-7			41	2.46 ± 0.05
long	L-1	2.7	154	9	0.73 ± 0.02
	L-2			11	0.92 ± 0.03
	L-3			15	1.23 ± 0.03
	L-4			18	1.45 ± 0.05
	L-5			22	1.72 ± 0.03
	L-6			25	1.93 ± 0.05
	L-7			30	2.24 ± 0.01
	L-8			33	2.53 ± 0.03

[a] Calculated from ^{1}H NMR data. [b] Measured by titration.

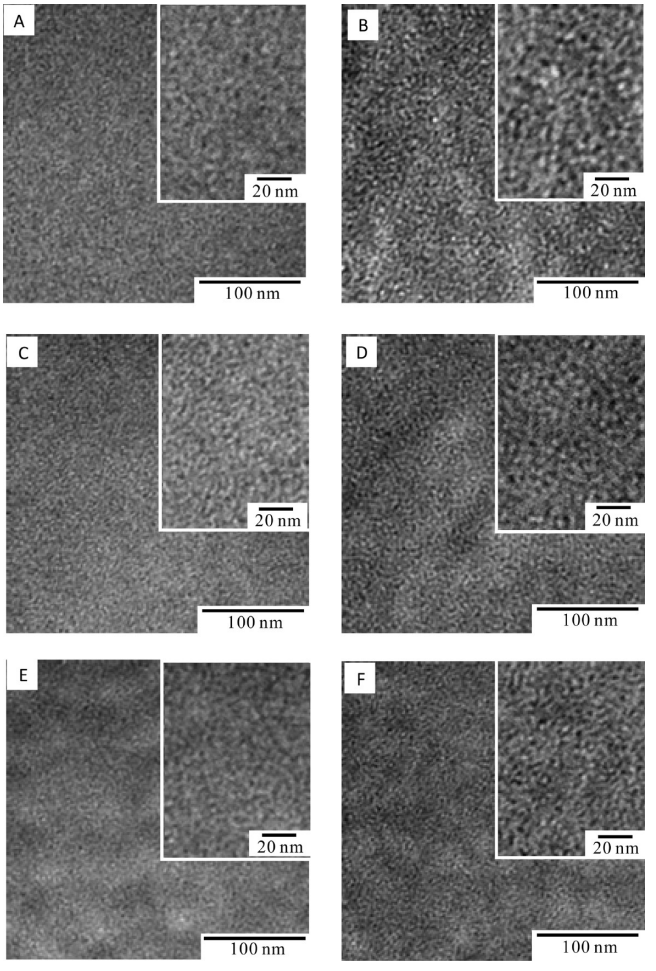

Figure 2. TEM images of P(VDF-*co*-CTFE)-*g*-SPS graft copolymer membranes: (A) S-1, IEC = 0.64 mmol/g; (B) S-6, IEC = 2.48 mmol/g; (C) M-1, IEC = 0.73 mmol/g; (D) M-7, IEC = 2.46 mmol/g; (E) L-1, IEC = 0.73 mmol/g; (F) L-8, IEC = 2.53 mmol/g.

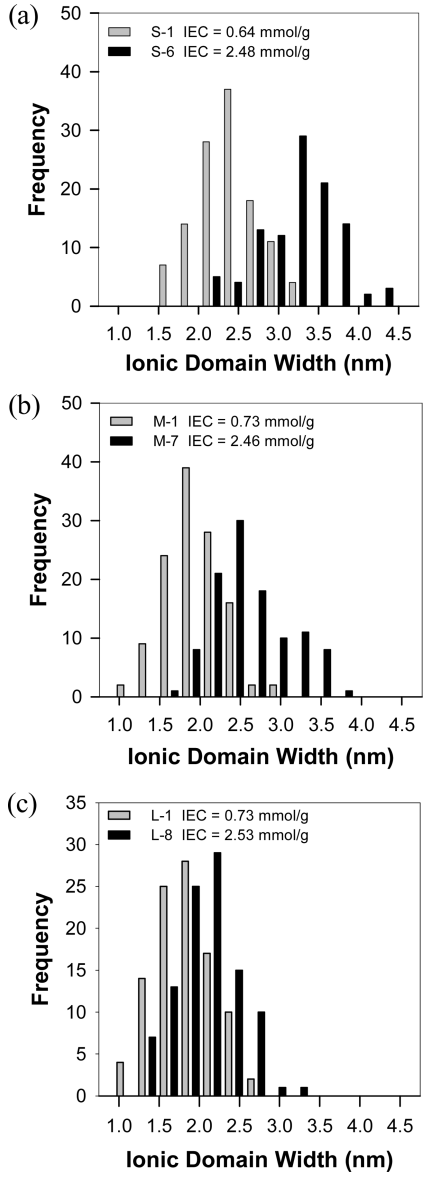

Figure 3. Distributions of the ionic cluster sizes in selected membranes from (a) short, (b) medium, and (c) long graft copolymer series.

hydrophobic regions. It was observed that all three series of the dry graft membranes possessed a phase-separated morphology characterized by small, 2−4 nm ionic clusters interconnected by narrow ionic channels. This morphology is very similar to that of Nafion, which possesses a "cluster network" comprised of 5−10 nm ionic clusters, but the dimensions are much smaller.[76−79]

In all three series of graft membranes, the ion content was observed to play an important role in phase separation and ionic aggregation. For each graft length series, membranes with lower IEC exhibit less distinctive phase separation wherein the interface between the ionic domains and the hydrophobic matrix is less sharp. On the other hand, in membranes with higher IEC, a more distinct phase-separated morphology with sharply visible ionic clusters is observed. In addition, the size of the ionic clusters increases with increasing IEC, which is explained on the basis of an increasing proportion of sulfonic acid ($-SO_3H$) groups present. Histograms showing the distribution of ionic cluster sizes in the membranes are presented in Figure 3, and the averaged data are summarized in Table 3. The ionic cluster

Table 3. Ionic Cluster Size and Number Density

membrane	IEC (mmol/g)	ionic cluster width (nm)	2-D cluster number density (per 1000 nm^2)
S-1	0.64	2.2 ± 0.4	21 ± 2
S-6	2.48	3.3 ± 0.4	19 ± 2
M-1	0.73	1.9 ± 0.3	26 ± 3
M-7	2.46	2.6 ± 0.4	28 ± 2
L-1	0.73	1.8 ± 0.3	25 ± 3
L-8	2.53	2.1 ± 0.3	35 ± 3

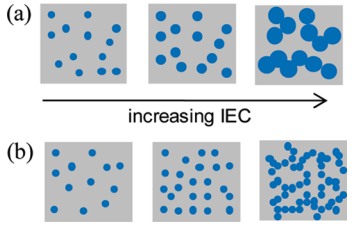

Figure 4. Schematic representation for the formation of a percolated ionic network: (a) increasing ionic cluster size but constant number of ionic clusters; (b) increasing number of ionic clusters but constant ionic cluster size.

size increases from 2.2 to 3.3, 1.9 to 2.6, and 1.8 to 2.1 nm over a similar IEC range of ~0.7 to ~2.5 mmol/g for membranes prepared from short, medium, and long graft length polymers, respectively. Moreover, the ionic cluster size shows a substantially larger increase with IEC for membranes prepared from the short graft length series. For instance, as IEC increases from 0.7 to 2.5 mmol/g, the ionic cluster size increases by 50% for the short graft series, whereas an increase of only 17% is observed for the long graft series. Furthermore, the number density of the ionic clusters is influenced by the ion content of the membranes, as summarized in Table 3. For the short graft membranes, the cluster number densities (measured in 2 dimensions) are 21 and 19 ± 2 clusters per 1000 nm^2 for the 0.7 and 2.5 mmol/g IEC samples, respectively. The cluster number density increases more significantly, from 25 to 35 clusters per 1000 nm^2, over a similar IEC range for the long graft membranes. The medium graft membranes show intermediate increases in number density upon increasing IEC. Thus, differences in the percolated ionic networks formed from polymers with different graft lengths are small but significant. Pictorially, these differences are depicted in Figure 4. For the short graft series, as IEC increases, the ionic cluster size increases while the number of ionic clusters remains approximately the same (Figure 4a). In contrast, for the long graft series, as the ion content increases, the number of ionic clusters increases but the ionic cluster size remains nearly constant (Figure 4b).

Intuitively, the ionic cluster size is expected to increase with increasing PS graft length. However, Figure 3 reveals the inverse is found to be true—membranes prepared from the shortest graft length series possessed larger ionic domains and, as graft length increases, the size of the ionic clusters decreases. This trend is accentuated for membranes possessing higher IEC. As summarized in Table 3, for membranes possessing IEC ~2.5 mmol/g, the average ionic cluster size decreases from 3.3 to 2.6 to 2.1 nm as the graft length transverses the series: short, medium, long. We believe this to be due to differences in the degree of sulfonation (DS) of the PS side chain: for a given IEC, a higher degree of sulfonation is required for the short graft copolymers because they inherently contain a lower styrene content. For instance, to achieve an IEC of ~2.5 mmol/g, the short graft

copolymers require a DS of 59%, whereas the long graft copolymers require only 33% (Table 2). A higher degree of sulfonation of the PS chains leads to a closer proximity between sulfonic acid groups along the graft chains. For example, for short graft copolymers possessing an IEC of 2.48 mmol/g (DS = 59%), every other styrene unit along the PS graft is sulfonated; in contrast, long graft copolymers, of IEC of 2.53 mmol/g (DS = 33%), possess poly(styrenesulfonic acid) groups that are separated by two non-sulfonated styrene units. The closer proximity of the sulfonic acid groups in the short graft copolymers relieves steric hindrance imposed from the intervening PS chain and allows stronger electrostatic attractions between the sulfonic acid groups to be formed, thus leading to larger and purer ionic aggregates.[80] By inference, if the ionic clusters are more ionically pure, the surrounding hydrophobic polymer in which they are embedded is more hydrophobically pure. In the case of the long graft copolymers, as more ions are introduced to the polymer, additional ionic clusters are being formed (increasing the cluster number density) because of the greater distances between the sulfonic acid groups and subsequent reduced electrostatic interactions; i.e., the formation of larger clusters is inhibited. The differences in ionic domain size, domain purity, and domain continuity have a strong influence on the membranes water sorption behavior, and hence proton conductivity, as will be shown later.

Water Sorption. The membranes' water sorption properties are expressed in terms of water content (wt % of water in a wet membrane) and molar ratio of water to sulfonic acid ($[H_2O]/[SO_3^-]$ or λ). Plots of water content versus IEC for the various series of P(VDF-*co*-CTFE)-*g*-SPS membranes are shown in Figure 5a. As expected, within each graft length series, water content increases with ion content. A similar trend is observed in the plot of λ vs IEC, as shown in Figure 5b. The water content and water uptake of Nafion 117 were measured to be 23% and 29%, respectively. For a similar IEC to Nafion 117 (IEC = 0.91 mmol/g), water sorption by the graft membranes (11−16 wt %) was significantly less.

Water content and water uptake are important parameters that provide insights into the continuity of the hydrophobic domains and the ability of the fluoropolymer matrix to resist osmotic pressure forces. Lower values of λ indicate stronger elastic forces of the fluoropolymer matrix and thus a greater ability to oppose osmotic pressure-driven swelling. When the osmotic pressure force exceeds the elastic forces of the matrix, dissolution occurs. The observation that the graft copolymer membranes absorb less water than Nafion reveals that the hydrophobic regions in the graft copolymers are well-interconnected and form a continuous network that allows exceedingly high IEC vinylic polymers to remain insoluble. A design feature found from this work is thus the continuous hydrophobic domain, facilitated by the formation of a high density of small nanosized ionic clusters, enhances the elastic forces in the matrix and limits excessive swelling of the membranes, allowing them to remain insoluble in water, even when the IEC is high.

To investigate the effects of graft chain length—and hence cluster size—on water sorption, membranes with similar IEC from different graft length series are compared. As shown in Figure 5a,b, the three membrane series exhibit very distinctive water sorption behavior that can be correlated to their graft lengths. For low IEC membranes (0.6−1.0 mmol/g), all three series absorb a similar amount of water regardless of the graft chain length. However, when IEC is increased beyond 1.0 mmol/g, the rate of increase of λ with IEC is considerably different for the three membrane series. For

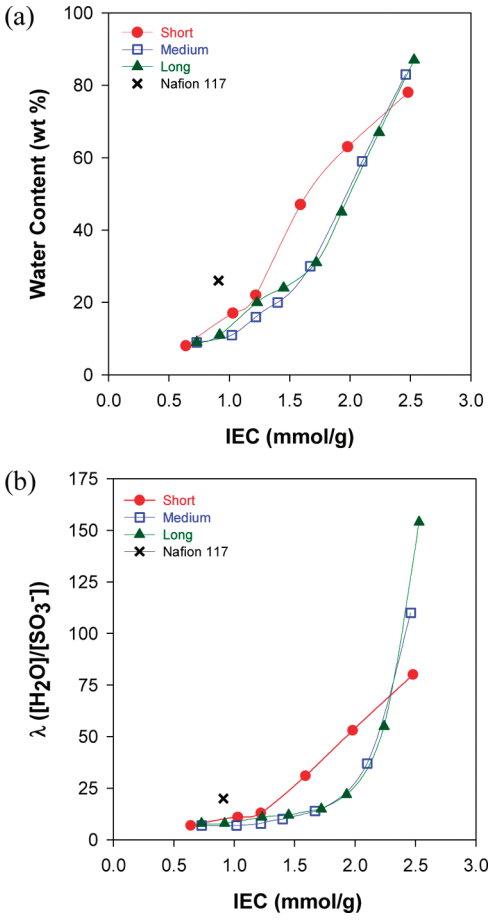

Figure 5. (a) Water content (wt %) vs IEC, (b) λ ($[H_2O]/[SO_3^{-2}]$) vs IEC for various series of P(VDF-*co*-CTFE)-*g*-SPS membranes: short (●), medium (□), and long (▲).

IECs ranging from 1.0 to 2.0 mmol/g, the short graft length series possess a much sharper increase in λ while the medium and the long series increase more steadily. Furthermore, the IEC threshold—beyond which water sorption increases sharply—is considerably lower for the short series (~1.20 mmol/g) than for the medium and the long series (~1.75 mmol/g). These results indicate that for intermediate IECs membranes with longer graft chain lengths are less vulnerable to swelling, but in the high IEC regime, i.e., where proton conductivity is high, membranes prepared from the shorter graft lengths are less susceptible to swelling. The molecular and morphological bases for these phenomena are discussed below.

According to Eisenberg, Hird, and Moore,[80] the morphology of random ionomers is characterized by formation of small ionic aggregates consisting of several ion pairs; these ionic aggregates are distributed randomly in a matrix of the host polymer. The formation of ionic aggregates is influenced by several factors, including the strength of the electrostatic interactions between ion pairs, the proximity of the ion pairs, the chain flexibility of the host polymer, and steric hindrances. Because the partially sulfonated polystyrene graft chains in P(VDF-*co*-CTFE)-*g*-SPS are essentially random ionomers, Eisenberg et al.'s[80] model can be used to explain the differences observed in the swelling behavior. As shown previously by TEM (Figure 2), membranes prepared from the short graft series possess larger ionic cluster sizes—which is rationalized as being due to a relatively higher degree of sulfonation and closer proximity of the sulfonic acid groups along the PS grafts. Since the sulfonic acid

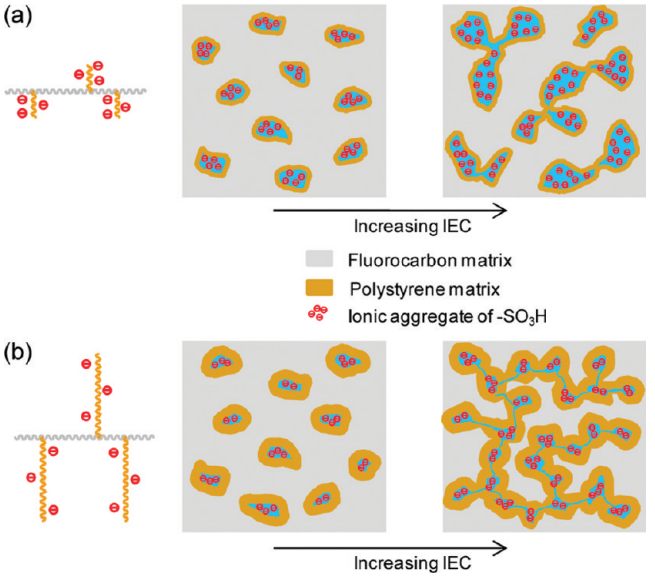

Figure 6. Schematic representation of the postulated ionic aggregation in P(VDF-*co*-CTFE)-*g*-SPS membranes with (a) short and (b) long graft length at different ion contents.

groups are more closely spaced, they experience greater electrostatic attractions among each other, resulting in larger ionic aggregates and more ionically pure domains, as illustrated in Figure 6a. Furthermore, the lower styrene content in the short graft copolymers causes the ionic aggregates to be surrounded by a thinner shell of hydrophobic polystyrene matrix, leading to a higher degree of water swelling in the low to intermediate IEC regime. The long graft membranes possess a relatively lower degree of sulfonation and more widely spaced sulfonic acid groups, resulting in smaller ionic aggregates (Figure 2). As the long graft polymers possess higher styrene content, these ionic aggregates are surrounded by a thicker shell of polystyrene matrix. This is schematically illustrated in Figure 6b. At low to intermediate IEC, it is postulated that the thicker layers of a polystyrene shell surrounding the ionic aggregates provide additional opposition to water swelling.

In the high (2.50 mmol/g) IEC regime, the trend in swelling is reversed. The short graft membrane exhibit significantly less swelling compared to the medium and the long graft membranes. TEM previously revealed that the short graft membranes exhibit a larger ionic cluster size as IEC increases, but the number of ionic clusters remains similar and relatively more isolated. This allows a more contiguous fluorocarbon matrix and, therefore, reduced water swelling in the high IEC regime (Figure 6a). In contrast, as IEC increases, membranes from the long graft series show an increase in the number of ionic clusters although the size of ionic cluster remains nearly constant. The increase in the density of ionic clusters leads to a smaller distance between ionic clusters and a more extensive percolation of ionic domains (Figure 6b). This in turn leads to greater water swelling in the long graft membrane at IEC of 2.50 mmol/g.

Wide-Angle X-ray Scattering. For Nafion membranes it is known that increasing the crystallinity can lead to lower water swelling due to an increase in the elastic energy of the polymer matrix.[81,82] In the present work, wide-angle X-ray scattering (WAXS) was performed to probe the structure at molecular length scales and to determine the degree of crystallinity in the membranes. The fluorinated backbone in the P(VDF-*co*-CTFE)-*g*-PS graft copolymers consists of

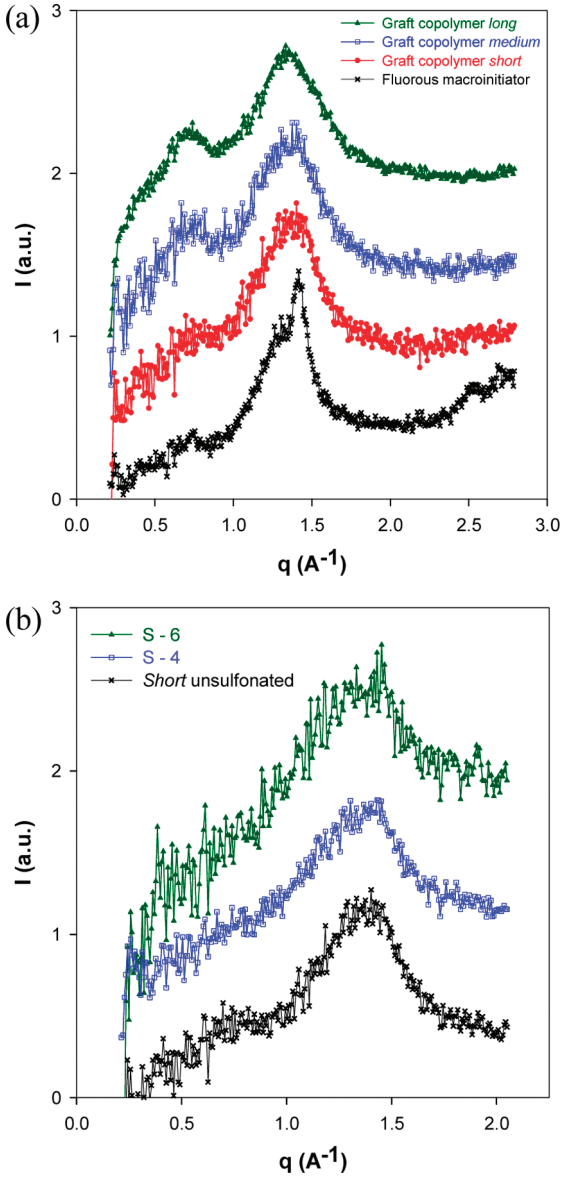

Figure 7. WAXS spectra for (a) membranes of P(VDF-*co*-CTFE) macroinitiator and P(VDF-*co*-CTFE)-*g*-PS graft copolymers of various graft lengths and (b) short graft membranes of various degree of sulfonation. Measured under ambient conditions. Intensity scale is in arbitrary units.

vinylidene difluoride (VDF) copolymerized with 5.8 mol % of chlorotrifluoroethylene (CTFE). Homopolymers of PVDF are highly crystalline polymers with poor solubility in common solvents.[83] Incorporation of the Cl atoms along the PVDF backbone perturbs the microstructural regularity, reduces crystallization, and results in improved solubility in common solvents. Figure 7a shows the WAXS spectra of membranes prepared from the P(VDF-*co*-CTFE) macroinitiator and the P(VDF-*co*-CTFE)-*g*-PS graft copolymers possessing various graft lengths. In the WAXS spectrum of the macroinitiator, the broad peak at a scattering wavevector q of 1.3 $Å^{-1}$, corresponding to a feature size of 4.8 Å, is associated with correlation distances between fluorinated polymer chains in the amorphous phase. A crystalline peak is observed on this broad peak, indicating a low degree of crystallinity. Two Gaussian peaks were fitted to the data to distinguish the crystalline peak from the broad amorphous peak and the percent of crystallinity, x_{cr}, was quantified using the ratio of scattering from the crystalline domains to

the overall scattering, as follows[84]

$$x_{cr} = \frac{I_{cr}}{I_{cr} + I_{am}} \quad (12)$$

where I_{cr} and I_{am} are the integrated signals of the crystalline and the amorphous peak, respectively. It was calculated that the percent of crystallinity in the P(VDF-*co*-CTFE) macroinitiator is 12 ± 1%.

In the WAXS spectra of the resultant P(VDF-*co*-CTFE)-*g*-PS graft copolymers, a broad peak is observed at a similar q range; however, the crystalline peak is either dramatically reduced or virtually absent. The percent of crystallinity is estimated to be 4 ± 2%, 2 ± 1%, and ~0% for the short, medium, and long graft copolymer membranes, respectively. The reduction in crystallinity can be considered to be due to steric hindrance of the polystyrene side chains which inhibits the crystallization of the fluorinated backbone. Since all three graft copolymers possessed poor crystallinity, the differences in water swelling between membranes with different graft lengths is unlikely to be due to differences in crystallinity. An additional broad peak at $q \sim 0.7$ Å^{-1}, corresponding to a feature size of 9 Å, is observed in the WAXS spectra of the graft copolymer membranes. We postulate that this peak is associated with the correlation distances between polystyrene chains since its intensity is increasing with increasing PS graft length.

The effect of sulfonation on crystallinity was also investigated. Figure 7b shows the WAXS spectra of the short graft membranes with various degrees of sulfonation. The percent of crystallinity was found to remain nearly constant (~4%) with increasing sulfonation. Similar observations (not shown) were found in membranes from the longer graft series. These results indicate that incorporation of $-SO_3H$ groups does not influence the crystallinity of the membranes, which is inherently low.

Proton Conductivity. In Figure 8a proton conductivity is compared for various series of P(CTFE-*co*-VDF)-*g*-SPS membranes as a function of IEC. As expected, within each series, proton conductivity generally increases with IEC. The critical IEC beyond which proton conductivity increases sharply with ion content is very similar for each series and occurs between 0.9 and 1.0 mmol/g.

For intermediate IECs (1.0−1.5 mmol/g), the short graft membranes show a sharper increase in proton conductivity with IEC. At high ion contents (IEC > 2.0 mmol/g), proton conductivities for all three series are observed to reach a maximum or even drop with further increase in IEC. This is due to the proportionally larger amounts of water absorbed at high ion contents, which leads to acid dilution. Figure 9a plots the acid concentration in hydrated membranes against IEC. It shows that membranes prepared from short graft polymers show a decrease in acid concentration as IEC increases above 1.20 mmol/g because these membranes swell to a greater extent in this IEC regime (Figure 5). The highest proton conductivity obtained in this work was observed in membrane from the long series (L-7: 0.095 S/cm at 2.24 mmol/g IEC); however, the "window" of IEC over which the *long* graft chain membranes exhibit relatively high proton conductivity is quite narrow because at low IEC they absorb too little water while at high IEC they absorb too much. In contrast, the IEC "window" of high conductivity increases for the medium and short series. For the very high IEC membranes (~2.50 mmol/g), it is the shorter graft chain polymers that provide the higher conductivity because in this region, the water content is relatively lower and the acid concentration is higher.

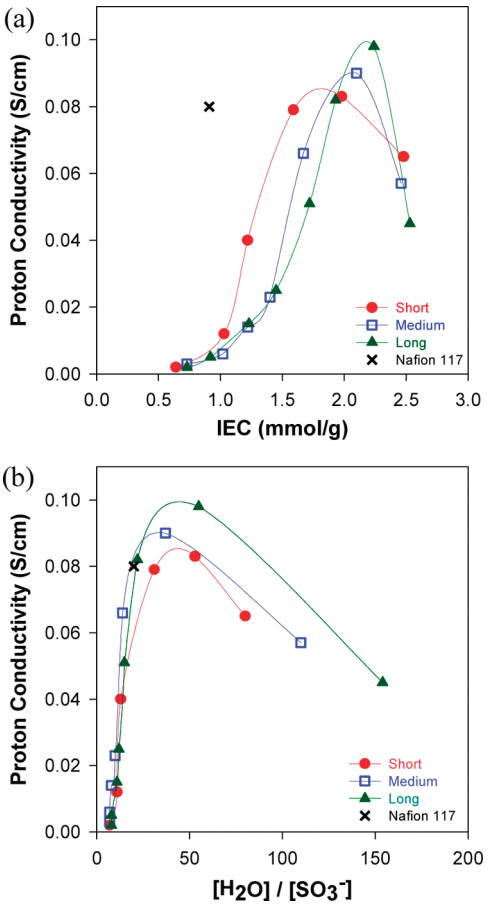

Figure 8. (a) Proton conductivity vs IEC and (b) proton conductivity vs $[H_2O]/[SO_3^-]$ for various series of P(VDF-*co*-CTFE)-*g*-SPS membranes: short (●), medium (□), and long (▲).

A deeper understanding of the observed trends in proton conductivity can be obtained by studying proton conductivity as a function of λ (Figure 8b). It is reported that the proton conductivity of perfluorosulfonic acid membranes increases significantly when λ values are >6.[85] Proton conductivity values for all three series are similar for λ values ranging between 10 and 15. At $\lambda > 20$, it can be seen that the ordering of conductivity is long > medium > short. The maximum conductivity values were observed in the region of $\lambda = 40-50$, which is similar to that observed for other polymer systems,[53] and serve as an empirical guideline in the design of proton conducting membranes.

The *effective* proton mobility, μ_{eff}, as derived from eq 7, allows the "normalized" proton conductivity to be determined; i.e., the effects of acid concentration on conductivity are removed. *Effective* proton mobilities provide useful insights into the extent of acid dissociation, ionic channel tortuosity, and spatial proximity of neighboring acid groups.[53] Figure 9b shows a plot of μ_{eff} versus IEC. Membranes prepared from short graft polymers possessed significantly greater proton mobility because these membranes possess higher water contents, which promote the dissociation of protons from the tethered sulfonic groups and form a more contiguous path for protons. A plot of μ_{eff} versus water volume fraction (X_v) is illustrated in Figure 9c. Proton mobilities appear independent of graft length but simply increase with water volume fraction until maximum value is reached. To remove the effects of the different acid strengths, the μ_{eff} was calculated at $X_v = 1.0$ by performing linear regressions and are summarized in Table 4. The μ_{eff} at

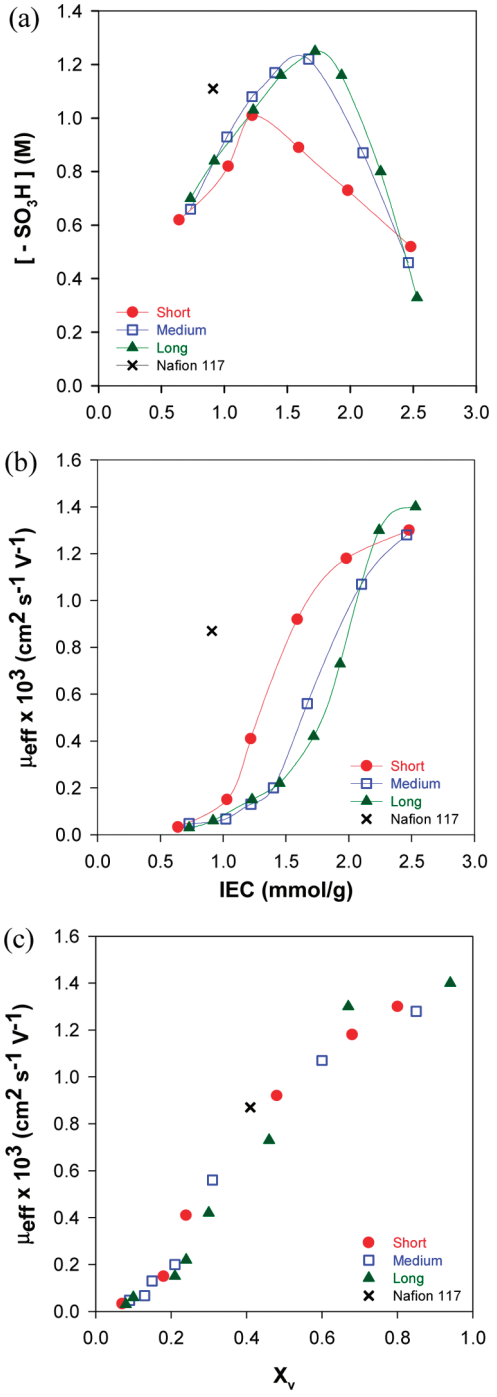

Figure 9. (a) Acid concentration in hydrated membranes vs IEC, (b) *effective* proton mobility (μ_{eff}) vs IEC, and (c) μ_{eff} vs water volume fraction (X_v) for various series of P(VDF-*co*-CTFE)-*g*-SPS membranes: short (●), medium (□), and long (▲).

$X_v = 1.0$ are 1.75×10^{-3}, 1.65×10^{-3}, and 1.66×10^{-3} cm^2 s^{-1} V^{-1} for short, medium, and long graft membranes, respectively. These mobility values are significantly lower than the theoretical mobility of a free proton in water at infinite dilution (3.63×10^{-3} cm^2 s^{-1} V^{-1} at 25 °C).[86] This may be a result of the tortuosity of the ionic pathways and the tethered $-SO_3^-$ groups. It is interesting to note that these μ_{eff} at $X_v = 1.0$ values are comparable to those of other PEM systems, i.e., 1.6×10^{-3}, 2.3×10^{-3}, and 2.6×10^{-3} cm^2 s^{-1} V^{-1} for BAM, Nafion, and poly(ethylene-*co*-tetrafluoroethylene)-*g*-poly(styrenesulfonic acid) [ETFE-*g*-PSSA], respectively.[87]

Table 4. Extrapolated Proton Mobility Values at Infinite Dilution ($X_v = 1.0$)

polymers	μ_{eff} at $X_v = 1.0$ ($\times 10^{-3}$ cm^2 s^{-1} V^{-1})	ref
short graft	1.75	this work
medium graft	1.65	this work
long graft	1.66	this work
BAM	1.6	84
Nafion	2.3	84
ETFE-*g*-PSSA	2.6	84

Conductivity as a Function of Temperature and Humidity. Proton conductivity of polymer electrolyte membranes is known to be dependent upon both temperature and water content,[3] and thus investigating how external conditions influence the conductivity is important for identifying the limitations of operation. Generally, for a given humidity, proton conductivity increases with temperature, and this is attributed to the activation barrier for proton motion, for which absorbed water is a highly influential factor. For example, the conductivity of Nafion 117 under 100% RH increases from 0.1 to 0.2 S/cm when the temperature is raised from 30 to 85 °C.[88] However, at higher temperature (> 90 °C), dehydration becomes a predominant factor and adversely affects proton conductivity. Furthermore, at a constant temperature, conductivity decreases as RH is decreased. In the case of Nafion 117, at 30 °C the conductivity decreases from 0.066 to 0.000 14 S/cm as RH decreases from 100% to 34%.[89]

In this section, conductivity data are presented for membranes prepared from long grafts with high IEC values (i.e., L-5, L-6, and L-7 possessing IECs of 1.72, 1.93, and 2.24, respectively). At ambient temperature and humidity, these membranes exhibit high proton conductivity (0.051−0.098 S/cm) and intermediate swelling (λ = 15−55) and high acid concentration (1.25−0.8 mol/L). It is therefore worthwhile to investigate their conductivity under various environmental conditions. As shown in Figure 10a, at a constant temperature of 30 °C, the conductivity of selected membranes increases with relative humidity, and since water sorption is directly related to the humidity, these data represent a change in conductivity with water content. At low RH (< 65%), dehydration of the membranes reduces the fraction of liquid-like water, leading to low conductivity (< 0.01 S/cm). Conductivity increases more sharply with RH for membranes with higher IEC. For instance, as RH increases from 75 to 95%, the conductivity increases from 0.016 to 0.089 S/cm for membrane L-7 (IEC = 2.24 mmol/g), whereas the conductivity increases steadily from 0.011 to 0.022 S/cm for membrane L-5 (IEC = 1.72 mol/g). This can be explained by the change in water uptake with relative humidity, as shown in Figure 10b. As expected, all three graft membranes, as well as Nafion 117, exhibit a substantial increase in water sorption with RH. However, the rate of increase in water uptake is significantly greater for membranes with higher IEC. For instance, for the RH range 75−95%, water uptake increases from 15 to 44% and from 10 to 25% for membranes L-7 and L-5, respectively. The dramatic increase in the water uptake of membrane L-7 is likely the cause of the sharp increase in proton conductivity with RH.

Figure 10c shows the relationship between proton conductivity and temperature for selected membranes prepared from long graft polymers, under 95% RH. The conductivity of the graft membranes (L-5, L-6, and L-7) and Nafion 117 increases with temperature to a maximum value, after which conductivity drops with further increase in temperature. The temperature at the maximum conductivity increases as the ion content increases. For instance, the maximum conductivity is observed at 50, 60, and 70 °C for membranes with

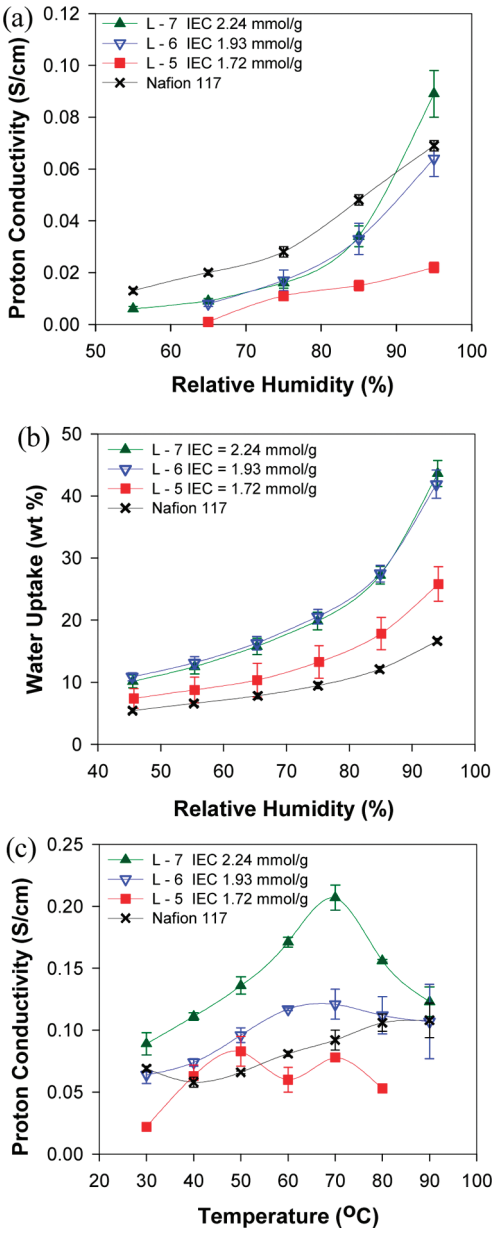

Figure 10. (a) Proton conductivity vs relative humidity, at 30 °C; (b) water uptake vs relative humidity, at 25 °C; and (c) proton conductivity vs temperature, at 95% RH, for P(VDF-*co*-CTFE)-*g*-SPS membranes from the long series and Nafion 117.

IEC of 1.72, 1.93, and 2.24 mmol/g, respectively. This indicates that graft membranes possessing higher ion content are less susceptible to dehydration and therefore exhibit a more continuous increase in conductivity over a greater temperature range.

From Arrhenius plots (not shown), the activation energy for proton transport are found to be 27.5, 17.3, and 18.3 kJ/mol for the graft membranes possessing IECs of 1.72, 1.93, and 2.24 mmol/g, respectively. These values are comparable with that found for Nafion 117, 14.1 kJ/mol (reported values are 7.8,[90] 9.6,[88] and 13.5[91] kJ/mol), and with the reported values of 12.9 kJ/mol for P(VDF)-*g*-SPS by Zhang et al.[72] The activation energies for proton conduction through P(VDF-*co*-CTFE)-*g*-SPS membranes show decreasing values (from 27.5 to 18.3 kJ/mol) as IEC increases. This observation agrees with the experimental data for P(VDF-*co*-HFP)-*b*-SPS diblock copolymer membranes where the activation energy is reported to fall from 25.7 to 17.1 kJ/mol as IEC increases from 0.72 to 1.18 mmol/g.[56] As shown previously in the TEM images, membranes with lower IEC form smaller, more isolated ionic clusters; thus, the energy barriers for both water swelling and proton motion are greater.

Conclusion

Partially sulfonated poly([vinylidene difluoride-*co*-chlorotrifluoroethylene]-*g*-styrene) [P(VDF-*co*-CTFE)-*g*-SPS] graft copolymers were devised and synthesized in order to systematically study the effects of graft chain length on PEM membrane properties. Three parent copolymers of P(VDF-*co*-CTFE)-*g*-PS were synthesized possessing similar graft density but different graft chains. Each of the three P(VDF-*co*-CTFE)-*g*-PS parent copolymers were sulfonated to different extents to provide three series of P(VDF-*co*-CTFE)-*g*-SPS membranes with various ion contents. All three parent graft copolymers possessed low crystallinity. The shorter graft length copolymer provided membranes with relatively larger ionic clusters although the cluster size in all the membranes was unusually small (2−4 nm)—much smaller than those found for Nafion (5−10 nm). The extent of sulfonation and the proximity of sulfonic acid groups along the polystyrene grafts are found to exert a role on the cluster size and, by inference, the ionic purity of the clusters. The formation of larger ionic clusters in the short graft series led to a greater water uptake in the low to intermediate IEC regime but the reverse for high IEC membranes. The lower degree of sulfonation and smaller ionic clusters found for long graft membranes led to a high fraction of hydrophobic polystyrene surrounding the ionic clusters, leading to lower swelling and higher acid concentration, although proton mobility was lower because of the lower extent of hydration. The smaller ionic cluster in the long graft membranes also allowed them to retain more water at low humidity conditions (2−3 times greater than that of Nafion) and maintain proton conduction at temperatures >70 °C and over wide humidity ranges. Research on the synthesis and characterization of fluorous−ionic graft copolymers with varied graft number density, and the effect on proton conductivity and morphology, is underway to further examine the structure−property relationships for this system. While it is recognized that sulfonated polystyrene-based systems may not be sufficiently stable under fuel cell operating conditions, this work clearly demonstrates that polymer microstructure, particularly graft length and sulfonic acid proximity, can be manipulated further to play a profound role in determining membrane morphology and ionic conductivity. These concepts should provide valuable insights into the design of PEMs for fuel cell applications.

Acknowledgment. This research was financially supported by the Natural Sciences and Engineering Research Council of Canada (NSERC). The authors thank Collin Zhang (SFU) and Dr. Andrew Lewis (SFU) for ^{19}F NMR measurement and Dr. Xu Han (SFU) and Zhongyuan Zhou (SFU) for their assistance with DMF-GPC.

Supporting Information Available: GPC traces, membrane properties, ^{1}H NMR, and ^{19}F NMR spectra. This material is available free of charge via the Internet at http://pubs.acs.org.

References and Notes

(1) Vielstich, W.; Lamm, A.; Gasteiger, H. A. *Handbook of Fuel Cells-Fundamentals, Technology and Applications*; Wiley: New York, 2003.
(2) Hickner, M. A.; Ghassemi, H.; Kim, Y. S.; Einsla, B. R.; McGrath, J. E. *Chem. Rev.* **2004**, *104*, 4587–4611.
(3) Rikukawa, M.; Sanui, K. *Prog. Polym. Sci.* **2000**, *25*, 1463–1502.
(4) Smitha, B.; Sridhar, S.; Khan, A. A. *J. Membr. Sci.* **2005**, *259*, 10–26.

(5) Li, Q.; He, R.; Jensen, J. O.; Bjerrum, N. J. *Chem. Mater.* **2003**, *15*, 4896–4915.
(6) Miyatake, K.; Watanabe, M. *Electrochemistry* (*Tokyo, Jpn.*) **2005**, *73*, 12–19.
(7) Hamrock, S. J.; Yandrasits, M. A. *Polym. Rev.* **2006**, *46*, 219–244.
(8) Heitner-Wirguin, C. *J. Membr. Sci.* **1996**, *120*, 1–33.
(9) Gursel, S. A.; Gubler, L.; Gupta, B.; Scherer, G. G. Radiation Grafted Membranes. In *Advances in Polymer Science*; Springer-Verlag: Berlin, 2008; Vol. *215*, pp 157−217.
(10) Qiu, X.; Li, W.; Zhang, S.; Liang, H.; Zhu, W. *J. Electrochem. Soc.* **2003**, *150*, A917–A921.
(11) Nasef, M. M.; Saidi, H.; Nor, H. M.; Foo, O. M. *Polym. Int.* **2000**, *49*, 1572–1579.
(12) Nasef, M. M.; Saidi, H.; Nor, H. M.; Foo, O. M. *J. Appl. Polym. Sci.* **2000**, *78*, 2443–2453.
(13) Arico, A. S.; Baglio, V.; Creti, P.; Di Blasi, A.; Antonucci, V.; Brunea, J.; Chapotot, A.; Bozzi, A.; Schoemans, J. *J. Power Sources* **2003**, *123*, 107–115.
(14) Ennari, J.; Hietala, S.; Paronen, M.; Sundholm, F.; Walsby, N.; Karjalainen, M.; Serimaa, R.; Lehtinen, T.; Sundholm, G. *Macromol. Symp.* **1999**, *146*, 41–45.
(15) Serpico, J. M.; Ehrenberg, S. G.; Fontanella, J. J.; Jiao, X.; Perahia, D.; McGrady, K. A.; Sanders, E. H.; Kellogg, G. E.; Wnek, G. E. *Macromolecules* **2002**, *35*, 5916–5921.
(16) Nacher, A.; Escribano, P.; Del Rio, C.; Rodriguez, A.; Acosta, J. L. *J. Polym. Sci., Part A: Polym. Chem.* **2003**, *41*, 2809–2815.
(17) Mokrini, A.; Del Rio, C.; Acosta, J. L. *Solid State Ionics* **2004**, *166*, 375–381.
(18) Mokrini, A.; Acosta, J. L. *Polymer* **2001**, *42*, 9–15.
(19) Kim, J.; Kim, B.; Jung, B. *J. Membr. Sci.* **2002**, *207*, 129–137.
(20) Elabd, Y. A.; Napadensky, E.; Walker, C. W.; Winey, K. I. *Macromolecules* **2006**, *39*, 399–407.
(21) Elabd, Y. A.; Napadensky, E.; Sloan, J. M.; Crawford, D. M.; Walker, C. W. *J. Membr. Sci.* **2003**, *217*, 227–242.
(22) Wei, J.; Stone, C.; Steck, A. E. 5422411, **1995**.
(23) Zaidi, S. M. J.; Mikhailenko, S. D.; Robertson, G. P.; Guiver, M. D.; Kaliaguine, S. *J. Membr. Sci.* **2000**, *173*, 17–34.
(24) Wang, F.; Hickner, M.; Kim, Y. S.; Zawodzinski, T. A.; McGrath, J. E. *J. Membr. Sci.* **2002**, *197*, 231–242.
(25) Ghassemi, H.; Ndip, G.; McGrath, J. E. *Polymer* **2004**, *45*, 5855–5862.
(26) Ghassemi, H.; McGrath, J. E.; Zawodzinski, T. A. *Polymer* **2006**, *47*, 4132–4139.
(27) Bauer, B.; Jones, D. J.; Roziere, J.; Tchicaya, L.; Alberti, G.; Casciola, M.; Massinelli, L.; Peraio, A.; Besse, S.; Ramunni, E. *J. New Mater. Electrochem. Syst.* **2000**, *3*, 93–98.
(28) Alberti, G.; Casciola, M.; Massinelli, L.; Bauer, B. *J. Membr. Sci.* **2001**, *185*, 73–81.
(29) Zhang, Y.; Litt, M.; Savinell, R. F.; Wainright, J. S.; Vendramint, J. *Polym. Prepr.* (*Am. Chem. Soc., Div. Polym. Chem.*) **2000**, *41*, 1561–1562.
(30) Zhang, Y.; Litt, M.; Savinell, R. F.; Wainright, J. S. *Polym. Prepr.* (*Am. Chem. Soc., Div. Polym. Chem.*) **1999**, *40*, 480–481.
(31) Genies, C.; Mercier, R.; Sillion, B.; Petiaud, R.; Cornet, N.; Gebel, G.; Pineri, M. *Polymer* **2001**, *42*, 5097–5105.
(32) Genies, C.; Mercier, R.; Sillion, B.; Cornet, N.; Gebel, G.; Pineri, M. *Polymer* **2001**, *42*, 359–373.
(33) Cornet, N.; Diat, O.; Gebel, G.; Jousse, F.; Marsacq, D.; Mercier, R.; Pineri, M. *J. New Mater. Electrochem. Syst.* **2000**, *3*, 33–42.
(34) Peron, J.; Ruiz, E.; Jones, D. J.; Roziere, J. *J. Membr. Sci.* **2008**, *314*, 247–256.
(35) Jones, D. J.; Roziere, J. *J. Membr. Sci.* **2001**, *185*, 41–58.
(36) Dang, T. D.; Bai, S. J.; Heberer, D. P.; Arnold, F. E.; Spry, R. J. *J. Polym. Sci., Part B: Polym. Phys.* **1993**, *31*, 1941–1950.
(37) Asensio, J. A.; Borros, S.; Gomez-Romero, P. *J. Polym. Sci., Part A: Polym. Chem.* **2002**, *40*, 3703–3710.
(38) Tang, H.; Pintauro, P. N. *J. Appl. Polym. Sci.* **2001**, *79*, 49–59.
(39) Wycisk, R.; Pintauro, P. N. Polyphosphazene Membranes for Fuel Cells. In *Advances in Polymer Science*; Springer-Verlag: Berlin, 2008; Vol. *216*, pp 157−183.
(40) Allcock, H. R.; Hofmann, M. A.; Ambler, C. M.; Lvov, S. N.; Zhou, X. Y. Y.; Chalkova, E.; Weston, J. *J. Membr. Sci.* **2002**, *201*, 47–54.
(41) Allcock, H. R.; Hofmann, M. A.; Ambler, C. M.; Morford, R. V. *Macromolecules* **2002**, *35*, 3484–3489.
(42) Kreuer, K. D. *J. Membr. Sci.* **2001**, *185*, 29–39.
(43) Yang, Y.; Holdcroft, S. *Fuel Cells* **2005**, *5*, 171–186.
(44) Gebel, G. *Polymer* **2000**, *41*, 5829–5838.
(45) Gebel, G.; Aldebert, P.; Pineri, M. *Polymer* **1993**, *34*, 333–339.
(46) Gebel, G.; Lambard, J. *Macromolecules* **1997**, *30*, 7914–7920.
(47) Rollet, A. L.; Diat, O.; Gebel, G. *J. Phys. Chem. B* **2002**, *106*, 3033–3036.
(48) Mauritz, K. A.; Moore, R. B. *Chem. Rev.* **2004**, *104*, 4535–4585.
(49) Rodgers, M. P.; Shi, Z. Q.; Holdcroft, S. *J. Membr. Sci.* **2008**, *325*, 346–356.
(50) Savard, O.; Peckham, T. J.; Yang, Y.; Holdcroft, S. *Polymer* **2008**, *49*, 4949–4959.
(51) Yang, Y. S.; Siu, A.; Peckham, T. J.; Holdcroft, S. Structural and Morphological Features of Acid-Bearing Polymers for PEM Fuel Cells. In *Advances in Polymer Science*; Springer-Verlag: Berlin, 2008; Vol. *215*, pp 55−126.
(52) Tsang, E. M. W.; Zhang, Z.; Shi, Z.; Soboleva, T.; Holdcroft, S. *J. Am. Chem. Soc.* **2007**, *129*, 15106–15107.
(53) Peckham, T. J.; Schmeisser, J.; Rodgers, M.; Holdcroft, S. *J. Mater. Chem.* **2007**, *17*, 3255–3268.
(54) Rodgers, M.; Yang, Y. S.; Holdcroft, S. *Eur. Polym. J.* **2006**, *42*, 1075–1085.
(55) Rubatat, L.; Shi, Z. Q.; Diat, O.; Holdcroft, S.; Frisken, B. J. *Macromolecules* **2006**, *39*, 720–730.
(56) Shi, Z. Q.; Holdcroft, S. *Macromolecules* **2005**, *38*, 4193–4201.
(57) Shi, Z. Q.; Holdcroft, S. *Macromolecules* **2004**, *37*, 2084–2089.
(58) Yang, Y. S.; Shi, Z. Q.; Holdcroft, S. *Macromolecules* **2004**, *37*, 1678–1681.
(59) Yang, Y. S.; Shi, Z. Q.; Holdcroft, S. *Eur. Polym. J.* **2004**, *40*, 531–541.
(60) Ding, J. F.; Tang, Q. Y.; Holdcroft, S. *Aust. J. Chem.* **2002**, *55*, 461–466.
(61) Ding, J. F.; Chuy, C.; Holdcroft, S. *Adv. Funct. Mater.* **2002**, *12*, 389–394.
(62) Ding, J. F.; Chuy, C.; Holdcroft, S. *Macromolecules* **2002**, *35*, 1348–1355.
(63) Ding, J. F.; Chuy, C.; Holdcroft, S. *Chem. Mater.* **2001**, *13*, 2231.
(64) Beattie, P. D.; Orfino, F. P.; Basura, V. I.; Zychowska, K.; Ding, J. F.; Chuy, C.; Schmeisser, J.; Holdcroft, S. *J. Electroanal. Chem.* **2001**, *503*, 45–56.
(65) Hillmyer, M. A.; Lodge, T. P. *J. Polym. Sci., Part A: Polym. Chem.* **2002**, *40*, 1–8.
(66) Radhakrishnan, K.; Switek, K. A.; Hillmyer, M. A. *J. Polym. Sci., Part A: Polym. Chem.* **2004**, *42*, 853–861.
(67) Zhang, M. F.; Russell, T. P. *Macromolecules* **2006**, *39*, 3531–3539.
(68) Gupta, B.; Scherer, G. G. *Angew. Makromol. Chem.* **1993**, *210*, 151–164.
(69) Flint, S. D.; Slade, R. C. T. *Solid State Ionics* **1997**, *97*, 299–307.
(70) Zhai, G. Q.; Ying, L.; Kang, E. T.; Neoh, K. G. *Macromolecules* **2002**, *35*, 9653–9656.
(71) Zhai, G. Q.; Kang, E. T.; Neoh, K. G. *J. Membr. Sci.* **2003**, *217*, 243–259.
(72) Zhang, Z. C.; Chalkova, E.; Fedkin, M.; Wang, C. M.; Lvov, S. N.; Komarneni, S.; Chung, T. C. M. *Macromolecules* **2008**, *41*, 9130–9139.
(73) Isbester, P. K.; Brandt, J. L.; Kestner, T. A.; Munson, E. J. *Macromolecules* **1998**, *31*, 8192–8200.
(74) Weiss, R. A.; Sen, A.; Willis, C. L.; Pottick, L. A. *Polymer* **1991**, *32*, 1867–1874.
(75) Xie, Z.; Song, C. J.; Andreaus, B.; Navessin, T.; Shi, Z. Q.; Zhang, J. J.; Holdcroft, S. *J. Electrochem. Soc.* **2006**, *153*, E173–E178.
(76) Ceynowa, J. *Polymer* **1978**, *19*, 73–76.
(77) Cheng, X.; Yi, B.; Han, M.; Zhang, J.; Qiao, Y.; Yu, J. *J. Power Sources* **1999**, *79*, 75–81.
(78) Rieberer, S.; Norian, K. H. *Ultramicroscopy* **1992**, *41*, 225–233.
(79) Xue, T.; Trent, J. S.; Osseoasare, K. *J. Membr. Sci.* **1989**, *45*, 261–271.
(80) Eisenberg, A.; Hird, B.; Moore, R. B. *Macromolecules* **1990**, *23*, 4098–4107.
(81) Park, Y. S.; Yamazaki, Y. *Polym. Bull.* **2005**, *53*, 181–192.
(82) Sacca, A.; Carbone, A.; Pedicini, R.; Portale, G.; D'Ilario, L.; Longo, A.; Martorana, A.; Passalacqua, E. *J. Membr. Sci.* **2006**, *278*, 105–113.
(83) Abbrent, S.; Plestil, J.; Hlavata, D.; Lindgren, J.; Tegenfeldt, J.; Wendsjo, A. *Polymer* **2001**, *42*, 1407–1416.
(84) Kasai, N.; Kakudo, M. *X-ray Diffraction by Macromolecules*; Kodansa Ltd.: Tokyo, 2005.
(85) Gavach, C.; Pamboutzoglou, G.; Nedyalkov, M.; Pourcelly, G. *J. Membr. Sci.* **1989**, *45*, 37–53.

(86) Adamson, A. A. *A Textbook of Physical Chemistry*; Academic Press: New York, 1973.
(87) Peckham, T. J.; Schmeissert, J.; Holdcroft, S. *J. Phys. Chem. B* **2008**, *112*, 2848–2858.
(88) Ma, C. S.; Zhang, L.; Mukerjee, S.; Ofer, D.; Nair, B. D. *J. Membr. Sci.* **2003**, *219*, 123–136.
(89) Anantaraman, A. V.; Gardner, C. L. *J. Electroanal. Chem.* **1996**, *414*, 115–120.
(90) Kopitzke, R. W.; Linkous, C. A.; Anderson, H. R.; Nelson, G. L. *J. Electrochem. Soc.* **2000**, *147*, 1677–1681.
(91) Halim, J.; Buchi, F. N.; Haas, O.; Stamm, M.; Scherer, G. G. *Electrochim. Acta* **1994**, *39*, 1303–1307.